Desalination and Water Treatment
www.deswater.com

doi: 10.1080/19443994.2015.1057036

57 (2016) 12902–12914
June

Taylor & Francis
Taylor & Francis Group

Compaction and relaxation of biofilms

R. Valladares Linares[a], A.D. Wexler[b], Sz.S. Bucs[a], C. Dreszer[b,c], A. Zwijnenburg[b], H.-C. Flemming[c], J.C. Kruithof[b], J.S. Vrouwenvelder[a,b,d,*]

[a]*Water Desalination and Reuse Center, Division of Biological and Environmental Science and Engineering, King Abdullah University of Science and Technology, Thuwal 23955-6900, Saudi Arabia, Tel. +31152782371; email: j.s.vrouwenvelder@tudelft.nl (J.S. Vrouwenvelder)*
[b]*Wetsus, European Centre of Excellence of Sustainable Water Technology, Oostergoweg 9, 8911 MA Leeuwarden, The Netherlands*
[c]*Biofilm Centre, University Duisburg-Essen, Universitätsstrasse 5, 45141 Essen, Germany*
[d]*Faculty of Applied Sciences, Department of Biotechnology, Delft University of Technology, Julianalaan 67, 2628 BC Delft, The Netherlands*

Received 20 April 2015; Accepted 27 May 2015

ABSTRACT

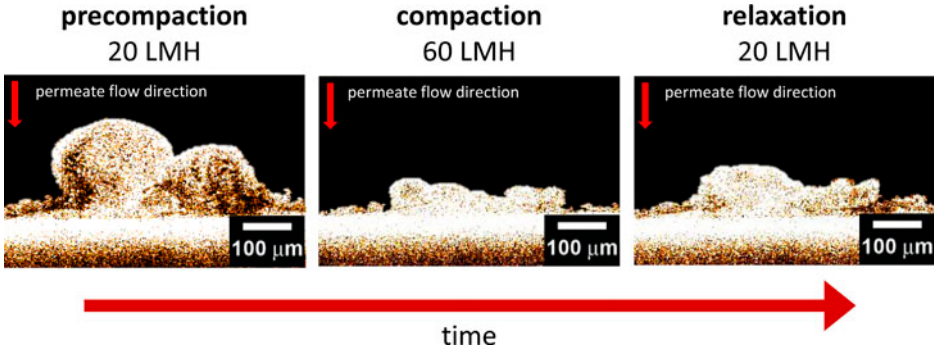

Operation of membrane systems for water treatment can be seriously hampered by biofouling. A better characterization of biofilms in membrane systems and their impact on membrane performance may help to develop effective biofouling control strategies. The objective of this study was to determine the occurrence, extent and timescale of biofilm compaction and relaxation (decompaction), caused by permeate flux variations. The impact of permeate flux changes on biofilm thickness, structure and stiffness was investigated *in situ* and non-destructively with optical coherence tomography using membrane fouling monitors operated at a constant crossflow velocity of 0.1 m s^{-1} with permeate production. The permeate flux was varied sequentially from 20 to 60 and back to 20 L m^{-2} h^{-1}. The study showed that the average biofilm thickness on the membrane decreased after elevating the permeate flux from 20 to 60 L m^{-2} h^{-1} while the biofilm thickness increased again after restoring the original flux of 20 L m^{-2} h^{-1}, indicating the occurrence of biofilm compaction and relaxation. Within a few seconds after the flux change, the biofilm thickness was

*Corresponding author.

changed and stabilized, biofilm compaction occurred faster than the relaxation after restoring the original permeate flux. The initial biofilm parameters were not fully reinstated: the biofilm thickness was reduced by 21%, biofilm stiffness had increased and the hydraulic biofilm resistance was elevated by 16%. Biofilm thickness was related to the hydraulic biofilm resistance. Membrane performance losses are related to the biofilm thickness, density and morphology, which are influenced by (variations in) hydraulic conditions. A (temporarily) permeate flux increase caused biofilm compaction, together with membrane performance losses. The impact of biofilms on membrane performance can be influenced (increased and reduced) by operational parameters. The article shows that a (temporary) pressure increase leads to more compact biofilms with a higher hydraulic resistance.

Keywords: Biofouling; Hydraulic biofilm resistance; Membrane filtration system; Biofilm thickness; Optical coherence tomography; Consolidation; Compression; Compressibility

1. Introduction

In the last decade, the use of membrane systems for fresh water production has increased strongly to supply the growing water demand due to increasing human population, industrial and agricultural activity, economic growth and urbanization [1]. When microorganisms are present in a non-sterile membrane system, biofilm formation takes place due to the availability of biodegradable nutrients in a continuous water flow through the system [2]. Biofilm formation is the accumulation of microorganisms, including extracellular compounds, on a surface due to either deposition or growth. Biofilms are ubiquitous on all surfaces in contact with non-sterile water. When biofilms are affecting membrane systems causing operational problems such as an unacceptable pressure drop increase, permeate flux reduction or salt passage increase, it is called biofouling [3].

An emerging phenomenon in biofilm studies is the consolidation of biofilms, which refers to possible structural realignment under dynamic conditions [4]. Structural deformation has been studied in biofilms grown under shear stress in pipelines [5]. It was concluded that *in situ* measurements of rheological properties of the biofilm (i.e. biofilm thickness) should be carried out under shear stress in order to produce representative results. Casey [6] proposed *compaction* as a mechanism contributing to the structural realignment of the biofilm under high shear force. *Compaction* is defined as the increase in density and the decrease in porosity of a biofilm, resulting in a thickness decrease of the biofilm. *Relaxation* is the opposite effect, defined as the decrease in biofilm density and the increase in porosity, resulting in a thickness increase. This behaviour of biofilms and its impact on performance losses is not yet fully understood.

Ohl et al. [7] investigated the effect of a varying fluid velocity on the density of heterotrophic biofilms grown for up to 80 d. Biofilms became more compact after increasing the flow velocity in the bulk liquid phase, while the biofilm density decreased when the flow velocity was reduced. The adaptation time of the biofilm thickness to new environmental conditions ranged between 1 and 3 weeks, depending on the initial biofilm thickness: a thick biofilm needed more time to adapt to new hydrodynamic conditions than a thin biofilm.

The mechanical compressibility of biofilms was investigated by applying a film rheometer [8] and by low load compression testing [9,10]. In both cases, a biofilm was grown on agar plates, transferred to the measuring device and compressed between two plates without a water flow. Studies by Dreszer et al. [11], performed in a transparent biofouling monitoring device, showed that the biofilm became thinner and the effect on membrane performance (measured by the biofilm resistance) became stronger when the crossflow velocity (linear flow velocity parallel to the membrane in $m\,s^{-1}$) was increased. Changes in the hydraulic biofilm resistance caused by a varying permeate flux ($l\,m^{-2}\,h^{-1}$ through the membrane) were reported by Dreszer et al. [12], applying a microfiltration membrane at which a biofilm was grown at constant crossflow velocity. Results showed that an increase of the permeate flux caused an increase in hydraulic biofilm resistance; while when the hydraulic biofilm resistance was reduced, the permeate flux was decreased. In other words, the effect of permeate flux on hydraulic biofilm resistance was reversible. Recently, Laspidou et al. [13] presented a biofilm model, in which compression of the biofilm resulted in the "closing" of voids making the biofilm material stiffer.

Optical coherence tomography (OCT) is a new technique to characterize membranes in water treatment applications and offers possibilities to investigate biofilms without addition of stains or signal enhancers which may affect the biofilm. OCT is an optical signal acquisition and processing method able to capture micrometre-resolution images from within optical scattering media during contact-free and non-invasive operation [14]. OCT enables production of two-dimensional (2-D) and three-dimensional (3-D) images of biofilms and has been used in a number of biofilm studies [15–21]. By application of a MATLAB algorithm on an OCT biofilm image, the biofilm thickness can be determined [15,16].

Derlon et al. [16] studied the formation of biofilms composed of metazoan organisms using OCT scans and showed the formation of open, spatially heterogeneous biofilms. The OCT results were compared to confocal laser scanning microscopy (CLSM) images of the same samples. Metazoans form a biofilm structure at meso- and macro-scale, and thus, CLSM observations at micro-scale provide only limited information compared to OCT scans, which can identify biofilm structures at both meso- and micro-scale. Xi et al. [19] concluded after studying biofilm development with *Pseudomonas aeruginosa* in standard capillary flow-cells that implementing OCT-related techniques enable the characterization of biofilm structure and function in more detail, particularly when studying the impact of flow dynamics, which have significant effects on biofilm structure and function.

The objective of this study was to determine the occurrence, extent and timescale of biofilm compaction and relaxation, and variations in hydraulic biofilm resistance caused by a change in permeate flux. The biofilm compaction and relaxation was characterized using real-time *in situ* 2-D OCT measurements. Microfiltration membranes (MF) were used to separate membrane from biofilm resistance. This study gives insight into the behaviour of biofilms in membrane systems and their effect on membrane performance in relation to operational parameters of membrane systems.

2. Material and methods

2.1. Membrane fouling simulator

A transparent membrane fouling simulator modified for *in situ* biofilm thickness measurements was used for this study. The transparent membrane fouling monitor is based on the membrane fouling simulator [22,23] developed for biofouling studies. Details of the used system (modified monitor) can be found in previous work [11,24]. Fig. 1 shows a picture of the monitor adapted for the OCT studies. The transparent monitor has a 4 cm × 15 cm × 0.4 cm-sized glass window on the monitor lid for imaging the biofilm on the membrane at various locations. The flow channel height of the monitor was 787 μm.

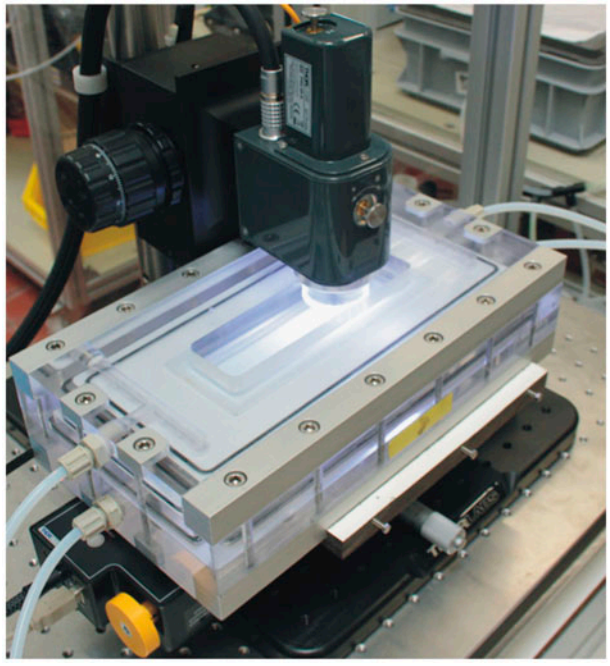

Fig. 1. Transparent membrane biofouling monitor modified for *in situ* biofilm thickness measurements with OCT. OCT measurements were performed during monitor operation at constant crossflow velocity (0.1 m s^{-1}) and permeate production (20 or 60 L m^{-2} h^{-1}). (adapted from Drezser et al. [11]).

2.2. Microfiltration membrane

The application of PES (polyethersulfone) MF (Nadir MP 005, Microdyn-Nadir GmbH Wiesbaden, Germany) with a pore size of 0.05 μm enabled low pressure operation and the investigation of biofouling/biofilm accumulation without any influence of concentration polarization or other types of fouling. Furthermore, membrane resistance and biofilm resistance could be clearly distinguished according to Dreszer et al. [12].

2.3. Feed water

Drinking water prepared from anaerobic groundwater (subsequently treated by aeration, rapid

sand filtration, deacidification, softening and rapid sand filtration at treatment plant Spannenburg in the Netherlands) is distributed without primary chemical disinfection and without a disinfectant residual. This drinking water was used as feed water source for the crossflow filtration system experiments. The feed water had a total bacterial cell number of 3×10^5 cells mL^{-1}. The number of colony forming units on R_2A media was 2×10^3 CFU mL^{-1} at 25°C after 10-d incubation. A concentrated nutrient solution was dosed into the feed water prior to the filtration cell at a flow rate of 0.12 L h^{-1}, using a peristaltic pump (Masterflex, Cole Parmer, Vernon Hills, USA). To restrict bacterial growth, the pH-value of the nutrient solution was set at 11 by sodium hydroxide addition. The dosing flow rate of the nutrient solution (0.12 L h^{-1}) was low compared to the feed water flow rate (28.3 L h^{-1}). Therefore, the high pH-value of the nutrient solution had no effect on the feed water pH of 7.8, and also no effect on the permeability. As nutrients, a solution of sodium acetate, sodium nitrate and sodium dihydrogen orthophosphate in the mass ratio for C:N:P of 100:20:10, respectively, was employed [25,26]. The concentration of sodium acetate added to the feed water was 1 mg L^{-1} of carbon, the amount of nitrogen and phosphorus was derived from the carbon concentration. Phosphate was dosed to avoid phosphate limiting conditions [27]. Fresh nutrient solutions were prepared every 2 d. All chemicals were purchased in analytical grade from Boom B.V. (Meppel, the Netherlands) and were dissolved in deionized water.

2.4. Measurements

2.4.1. Optical coherence tomography (OCT)

In situ imaging of the feed channel surface of the membrane was performed using a spectral domain optical coherence tomograph (Thorlabs Ganymede OCT System). The OCT was fitted with a 5 × telecentric scan lens (Thorlabs LSM03BB) which provides a maximum scan area of 100 mm^2. The OCT engine was configured to provide high-resolution images with a sensitivity of 106 dB at 1.25 kHz A-scan rate. Volumetric images were created using the maximum intensity profile algorithm included in the instrument software (Thorlabs SD-OCT system software version 3.2.1) for a rectangular area of 2 mm × 5 mm using 200 B-scans and 500 A-scans of 619 pixels corresponding to a physical depth of 1.1 mm. Image processing details can be found in previous publications [11,15,16].

2.4.2. Thickness

Biofilm thickness was calculated based on the number of pixels found between the top edge of the biofilm and the upper membrane surface of each OCT image, using a pixel scaling factor to obtain the biofilm thickness in microns. Biofilm thickness change rate was calculated based on the average measurements of the biofilm thickness in time intervals of 100 ms, which determines the variation of biofilm thickness in time. Biofilm thickness range was calculated for the total OCT scanned areas, limited in value by the thickest and thinnest sections of the biofilm in the scan. Biofilm stiffness was defined as the variation in time of biofilm thickness of a single scan area measured 10 times in series. A small variation in thickness indicates a high biofilm stiffness, while a large variation in thickness indicates a low biofilm stiffness.

2.5. Experimental conditions

Feed water was filtered through two 10-μm pore size cartridge filters, and the temperature was kept constant at 20°C. A pressure reducer (V782, Vink Kunststoffen B.V., Didam, the Netherlands) enabled a stable feed pressure of 1.7 bar. Before the water entered the filtration cell, nutrients were added. The linear flow velocity of the feed water was monitored by a flow controller (8805/8905, Brooks Instrument, Hatfield, PA, USA) installed behind the outlet of the monitor. The permeate rate (flux) was maintained by

Table 1
Structure of studies performed with the transparent membrane biofouling monitor

	Sections	Figures
Validation studies	3.1	
Hydraulic characterization of the monitor	3.1.1	Fig. 2
Flow field distribution	3.1.2	Fig. S1
Use of microfiltration membrane (superficial fouling)	3.1.3	Fig. 3, S2
Effect of flux on hydraulic biofilm resistance	3.2	Fig. 4
Compaction and relaxation of the biofilm	3.3	
Biofilm thickness	3.3.1	Fig. 5
Biofilm thickness change rate	3.3.2	Figs. 6, 7
Biofilm thickness range	3.3.3	Fig. 8(a)
Biofilm stiffness	3.3.4	Fig. 8(b)

Note: Figs. S1 and S2 are shown in the Supplementary material section.

a peristaltic pump (Masterflex L/S pumps, Cole-Parmer Instrument Company, Vernon Hills, Illinois, USA). The fouling development was monitored by measuring the pressure drop over the feed channel and over the membrane, using a differential pressure transmitter (Deltabar S PMD70, Endress + Hauser, Maulburg, Germany; (Vrouwenvelder et al. [25])). The pressures were measured at the monitor inlet, permeate and concentrate outlet. Temperature, flow velocity, flux, feed channel pressure drop (FCP), transmembrane pressure drop (TMP) and nutrient supply were measured twice a day. Transmembrane and biofilm resistance data were calculated as described by Dreszer et al. [12].

The monitor was operated at a crossflow velocity of 0.10 m s^{-1} and a permeate flux of 20 L m^{-2} h^{-1} without a feed spacer. To enhance biofilm accumulation, the feed water was supplemented with a carbon concentration of 1 mg L^{-1}. Table 1 shows the structure of the studies performed to validate the monitor representativeness for practice, to investigate the effect of permeate flux changes on the biofilm structure and to show the compaction and relaxation behaviour of biofilms.

To assess the effect of flux changes on hydraulic biofilm resistance and during compaction and relaxation experiments, the regular permeate flux was set to 20 L m^{-2} h^{-1}; to compact the biofilm, the permeate flux was subsequently increased to 60 L m^{-2} h^{-1} for 1 h, and then restored to 20 L m^{-2} h^{-1} for the biofilm relaxation period. All these experiments were performed on a biofilm pregrown for 4 d at a permeate flux of 20 L m^{-2} h^{-1} and a crossflow velocity of 0.10 m s^{-1}.

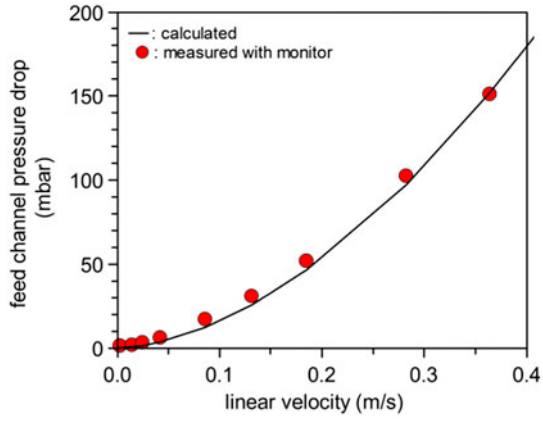

Fig. 2. Feed channel pressure drop (mbar) as a function of the linear velocity (m s^{-1}) in the transparent membrane biofouling monitor containing a feed spacer. Calculated data using Schock and Miquel (1987) equation for spiral-wound membrane elements (adapted from Dreszer et 'al. [24]).

3. Results

Validation studies were performed with the transparent membrane biofouling monitor modified for *in situ* OCT biofilm thickness measurements to evaluate the membrane and monitor performance and the suitability for the study (Section 3.1). Afterwards, the effect of permeate flux changes on hydraulic biofilm resistance (Section 3.2) and on compaction and relaxation of the biofilm (Section 3.3) were assessed.

3.1. Validation studies

Validation studies were performed on hydraulic characterization (Section 3.1.1), flow field distribution along the monitor (Section 3.1.2) and the growth of a biofilm on the surface of a microfiltration membrane (Section 3.1.3).

3.1.1. Hydraulic characterization of the monitor

Fig. 2 shows the feed channel pressure drop as a function of the linear velocity in the monitor, based on measured data in the system and calculated data by applying the mathematical model proposed by Schock and Miquel [28]. A good correlation between both sets of data was observed, confirming that the monitor has

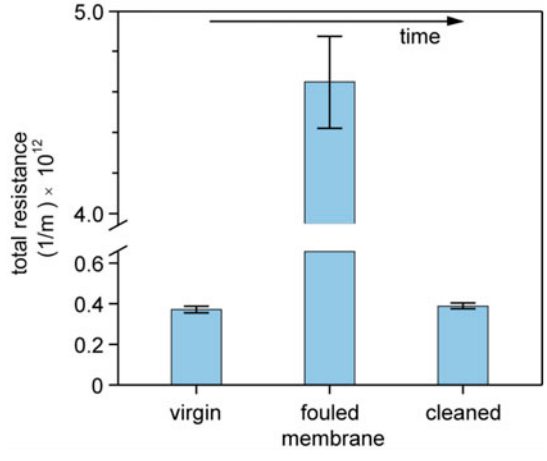

Fig. 3. Total resistance prior to fouling (virgin membrane), after fouling and after subsequent cleaning by scraping of the fouled membrane surface to remove the accumulated biofilm. A similar resistance of the virgin and cleaned membrane indicates that fouling predominantly occurred on the membrane surface (adapted from Dreszer et al. [12]). See Fig. S2 in supplementary material for additional data on the biofilm localization.

similar spatial dimensions as a spiral-wound membrane element (i.e. feed spacer channel height).

3.1.2. Flow field distribution

The flow field distribution was assessed by visual observations using the glass sight window of the monitor (Fig. 1). The test involved the injection of a blue dye into the feed water to determine the distribution of the water flow along the monitor in time. Fig. S1 in supplementary material shows a homogeneous flow distribution over the monitor width. The hydraulic characterization of the monitor (Fig. 2) and the flow field distribution (Fig. S1 in supplementary material) showed the monitor's suitability for the studies.

3.1.3. Microfiltration membrane use

A 0.05-μm pore size microfiltration membrane was used to enable the biofilm growth under low pressure conditions and to avoid salt concentration polarization. The system was fed with tap water (dosed with 1 mg L^{-1} acetate C as biodegradable substrate) at a crossflow velocity of 0.10 m s^{-1}, maintaining a constant water permeate flux through the membrane of 20 L m^{-2} h^{-1}. After 4 d of operation, scanning electron microscopy (SEM) cross section images of the fouled membrane (Fig. S2 in supplementary material) revealed that the biofilm layer was formed on the membrane surface only and not inside the pores of the membrane.

Fig. 3 presents the membrane resistance of a virgin, fouled and mechanically cleaned membrane. The results show that the fouling predominantly occurred on the membrane surface, since the mechanical scrubbing of the fouling resulted in a membrane resistance only slightly (5%) higher than the resistance of the virgin membrane. The biofilm resistance measurements and SEM imaging both showed that fouling mainly occurred on the membrane surface and that the selected microfiltration membrane is suitable for the studies.

3.2. Effect of flux change on hydraulic biofilm resistance

The hydraulic resistance of the biofilm was assessed for two different permeate flux regimes: (i) an original permeate flux of 20 L m^{-2} h^{-1} was increased to 60 L m^{-2} h^{-1} and lowered again to 20 L m^{-2} h^{-1}; (ii) a permeate flux of 60 L m^{-2} h^{-1} was lowered to 20 L m^{-2} h^{-1} and increased again to 60 L m^{-2} h^{-1}. Permeate flux was changed after the hydraulic resistance and biofilm thickness was stabilized.

The results for the hydraulic biofilm resistance are shown in Fig. 4 for both experiments. There was a strong increase in biofilm resistance after elevating the permeate flux from 20 to 60 L m^{-2} h^{-1}. When the flux was lowered again to the original value (20 L m^{-2} h^{-1}), the biofilm resistance decreased again, showing a dynamic reversible process. Restoring the original permeate flux did not reinstate the initial hydraulic biofilm resistance completely; the final hydraulic resistance was 16% higher than the initial one.

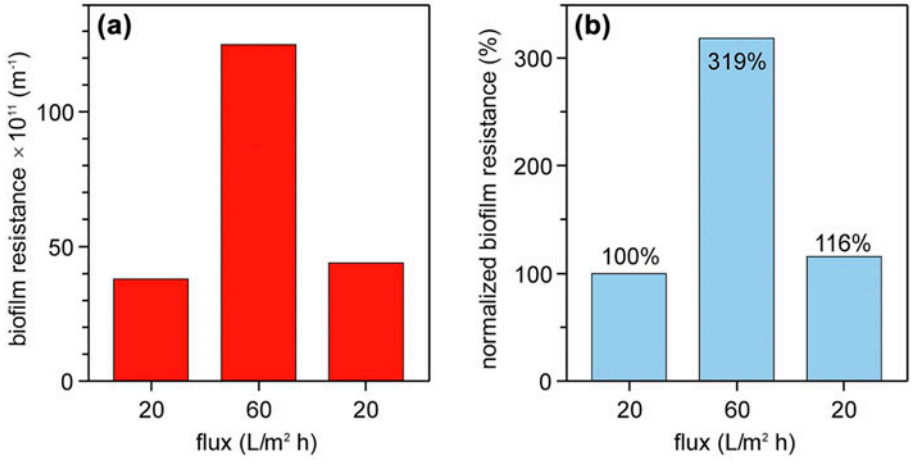

Fig. 4. (a) Hydraulic biofilm resistance and (b) normalized biofilm resistance at a permeate flux of 20 L m^{-2} h^{-1}, after permeate flux increase to 60 L m^{-2} h^{-1}, and after restoring the original flux of 20 L m^{-2} h^{-1}. The crossflow velocity was constant: 0.10 m s^{-1}. (Dreszer et al. [11]).

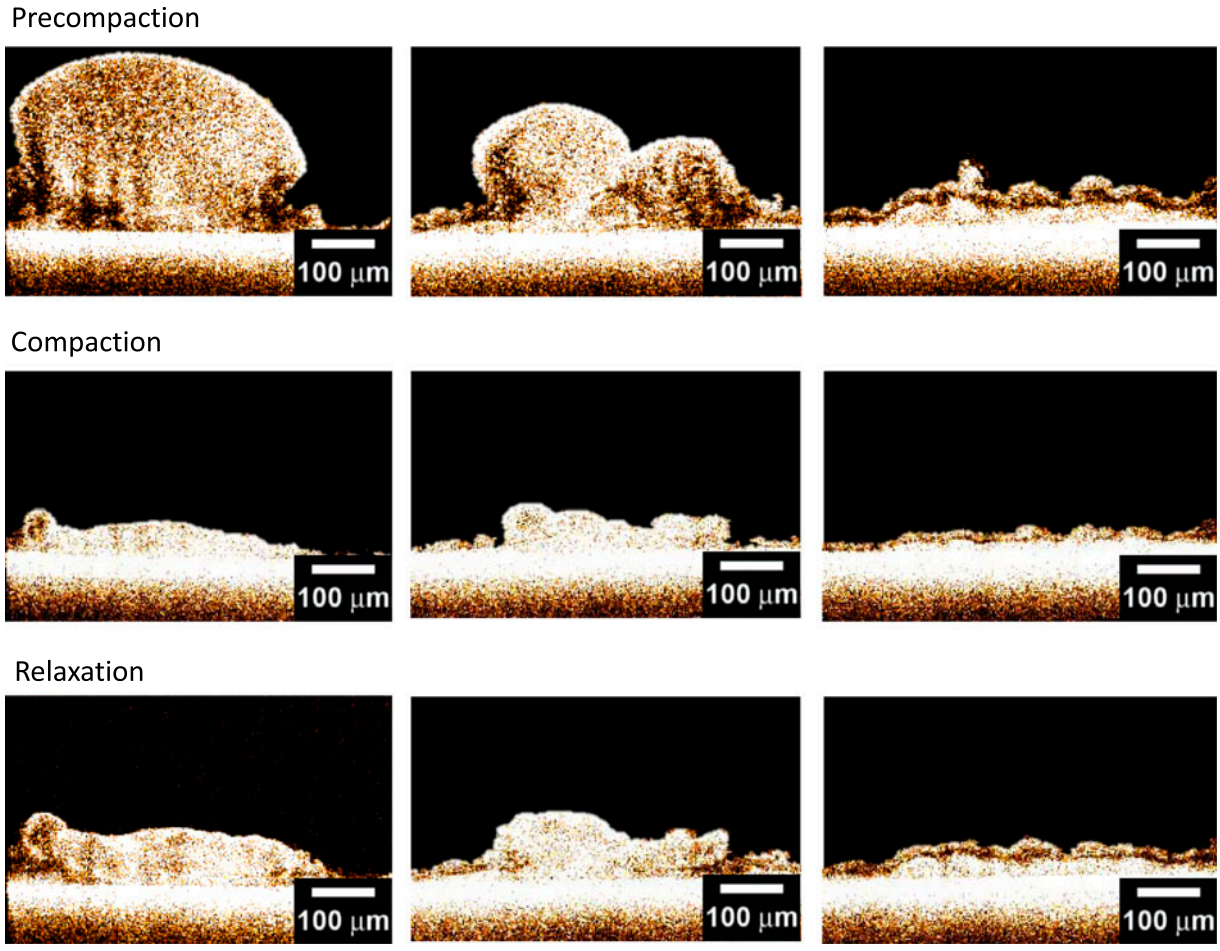

Fig. 5. OCT observations of the biofilm at three different locations at permeate flux 20 L m^{-2} h^{-1} (precompaction), after flux increase to 60 L m^{-2} h^{-1} (compaction), and after restoring the original flux of 20 L m^{-2} h^{-1} (relaxation). The lateral scan length is 8 μm. The images were made at a constant crossflow velocity (0.10 m s^{-1}).

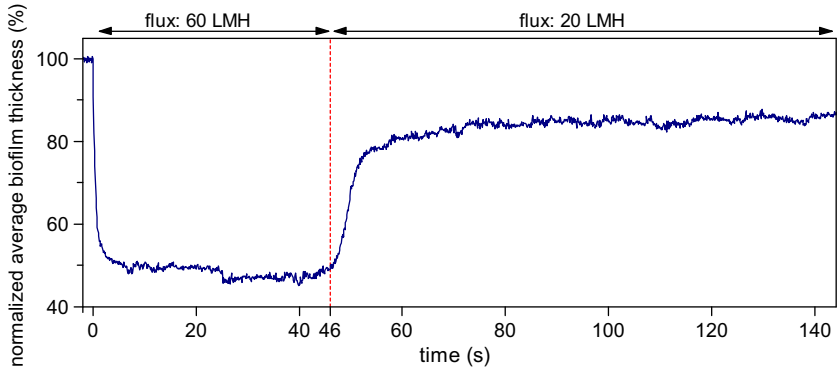

Fig. 6. Average biofilm thickness in time after increasing the permeate flux (from 20 to 60 L m^{-2} h^{-1}) and restoring the original flux (from 60 to 20 L m^{-2} h^{-1}) determined with OCT. Individual frames (B-scans) from the sequence were taken at intervals of 100 ms, for each 255 pixels (A-scans). The crossflow velocity was constant: 0.10 m s^{-1}.

In the next section of this article, the research is described how this reversible increase and decrease of hydraulic biofilm resistance is related to the biofilm thickness and/or to the biofilm compaction and relaxation behaviour.

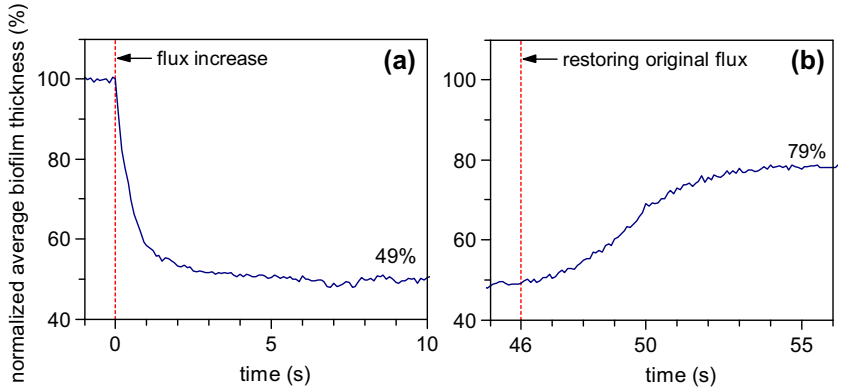

Fig. 7. Normalized average biofilm thickness in time. (a) directly after increase in permeate flux from 20 to 60 L m^{-2} h^{-1} and (b) directly after restoring the original permeate flux from 60 to 20 L m^{-2} h^{-1}.

3.3. Compaction and relaxation of the biofilm

The behaviour of the biofilm (compaction and relaxation) under varying permeate fluxes was analysed with OCT scans, and then related to variation in the biofilm thickness, biofilm thickness change rate and biofilm stiffness. For this, the permeate flux was first set to 20 L m^{-2} h^{-1}, then increased to 60 L m^{-2} h^{-1} until the biofilm thickness stabilized and then lowered again to 20 L m^{-2} h^{-1}.

3.3.1. Biofilm thickness

Fig. 5 shows OCT scans for three locations of the membrane, with a biofilm present on the membrane surface. The scans for the precompaction phase, taken at a permeate flux of 20 L m^{-2} h^{-1}, showed a smooth, fluffy and mushroom-like biofilm structure. During the compaction stage, where the flux was increased to 60 L m^{-2} h^{-1}, the biofilm was compressed to 49% of the original thickness (see Fig. 6 for the average biofilm thickness in time). After the biofilm thickness stabilized, the flux was restored to 20 L m^{-2} h^{-1}. This caused an increase of the biofilm thickness to 79% of the original thickness. The original biofilm thickness was not fully restored, but a significant thickness increase was observed in the relaxation stage. A stepwise change in hydrodynamic conditions (increase/decrease of permeate flux) changed the structural properties of the biofilm, resulting in the compaction or relaxation of the biofilm.

3.3.2. Biofilm thickness change rate

Measurements of the average biofilm thickness were made after time intervals of 100 miliiseconds (ms).

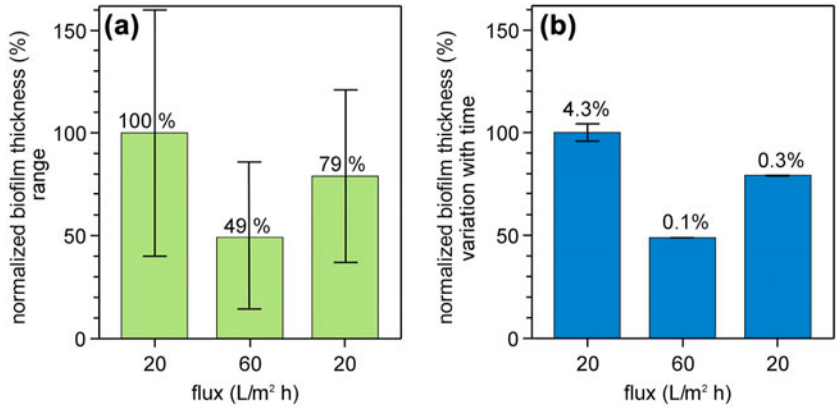

Fig. 8. (a) Normalized biofilm thickness range and (b) normalized biofilm thickness variation in time during 10 repetitive thickness measurements at a permeate flux of 20 L m^{-2} h^{-1}, after permeate flux increase to 60 L m^{-2} h^{-1}, and after restoring the original flux to 20 L m^{-2} h^{-1}. The bars in (a) show the total range of biofilm thickness in the total OCT scan area. The bars in (b) show the thickness variation for ten measurements in series with time in a single OCT scan area. The crossflow velocity was constant: 0.10 m s^{-1}.

Fig. 6 shows the normalized values for the thickness in time for the 2 flow regimes: (i) increasing the permeate flux from 20 to 60 L m^{-2} h^{-1} at $t = 0$ s and restoring the original flux from 60 to 20 L m^{-2} h^{-1} after 46 s until the end of the experiment after 145 s. Fig. 7 shows the compaction and relaxation processes for the first 10 s after a flux change. During compaction after the permeate flux was increased to 60 L m^{-2} h^{-1}, in approximately 2 s the average biofilm thickness decreased to 49% of the initial value (Fig. 7(a)). After the flux increase, biofilm compaction was strongest during the first 0.1 s and thereafter a gradual biofilm thickness decline was found for about 1 s, after which the thickness remained constant. From Fig. 7(b), it can be seen that when the flux was restored to 20 L m^{-2} h^{-1}, the biofilm thickness regained 79% of the original precompaction thickness in a time s of approximately 10 s. Biofilm relaxation showed a slower and more gradual thickness increase in time compared to the thickness decline during compaction (Fig. 7). Replicate experiments confirmed the results of the study.

The biofilm thickness change rate for compaction and relaxation differed, while restoring the original flux did not completely restore the original biofilm thickness. Biofilm compaction showed to be faster than biofilm relaxation.

3.3.3. Biofilm thickness range

The *biofilm thickness range in the total OCT scan area* at constant permeate flux was determined at subsequently a flux of 20, 60 and 20 L m^{-2} h^{-1} (Fig. 8(a)). The normalized biofilm thickness range in the scan area varied significantly. At the permeate flux of 20 L m^{-2} h^{-1} prior to compaction (i) the biofilm thickness varied from about 40 to 160% of the average biofilm thickness and (ii) the total membrane surface was covered with a biofilm (Fig. 8(a): left bar). After the flux increase, the average, minimal and maximum thickness decreased (varying from about 11 to 87% of the average thickness at initial permeate flux), indicating a reduction in both the average biofilm thickness and the range of biofilm thickness over the total scan area (Fig. 8(a): left and centre bar). When the flux was restored back to 20 L m^{-2} h^{-1}, the average, minimal and maximum biofilm thickness increased (varying from about 35 to 123% of the original average biofilm thickness). However, the thickness range was not fully restored to the original thickness range found prior to the flux increase. The shift of the biofilm thickness range in the total OCT scan area with permeate flux change show that compaction and decompaction occurred for thin and thick biofilms.

3.3.4. Biofilm stiffness

The *variation in time of the biofilm thickness* of a single OCT scan area measured 10 times for precompaction, compaction and relaxation is shown in Fig. 8(b). At a permeate flux of 20 L m^{-2} h^{-1} prior to compaction, the biofilm thickness varied 4.3% with time. After the flux increase, the biofilm thickness variation in time was strongly reduced (from 4.3 to 0.1%), illustrating that the biofilm thickness was more constant in time. When the flux was restored to 20 L m^{-2} h^{-1}, the biofilm thickness variation in time remained low (0.3%) compared to prior the permeate flux increase (4.3%). The biofilm structure became more rigid (less thickness variation with time) during and after biofilm compaction caused by a permeate flux increase.

4. Discussion

The main objective of this study was to analyse the compaction and relaxation behaviour of a biofilm grown on the surface of a microfiltration membrane using a monitor operated at a constant crossflow velocity (0.10 m s^{-1}) with variable permeate flux. OCT was used as a non-destructive imaging technique. The impact of water permeate flux changes on biofilm thickness (Fig. 5), biofilm thickness change rate (Figs. 6 and 7), biofilm thickness range (Fig. 8(a)), and biofilm stiffness (Fig. 8(b)) was studied. An increase in permeate flux (from 20 to 60 L m^{-2} h^{-1}) resulted in a decrease in biofilm thickness and an increase of biofilm stiffness. Restoring the original permeate flux did not completely restore the original biofilm thickness, biofilm stiffness and hydraulic biofilm resistance, suggesting a relation between these biofilm parameters and membrane performance. Biofilm compaction and relaxation occurred in a timescale of seconds.

4.1. Impact of biofilm compaction and relaxation

The impact of compaction and relaxation of biofilms has been reported based on density and biofilm resistance measurements. In particular, the effect of: (i) higher shear stress due to increased crossflow velocity in the feed channel [7] and (ii) increased permeate flux through the membrane [11] has been studied. A change in biofilm thickness can be caused by a change in the concentration and properties of the biofilm extracellular polymeric substances (EPS) and/or the biofilm void volume. Comparing the OCT scans (Fig. 5) before and after compaction shows the collapse of small mushroom-like biofilm structures during the flux increase, suggesting the presence of local

voids in the biofilm during the precompaction stage. The variation in the EPS concentration and the elastic properties of the EPS [29] cannot be analysed by OCT scans. The elasticity of polymers in the EPS may be accountable for compaction and relaxation behaviour of the biofilm [29–31]. Laspidou et al. [13] showed that biofilm voids change in the deforming biofilm and that consolidation plays an important role in the mechanical properties, making old and consolidated biofilms overall stiffer. This study showed that compaction and subsequent relaxation of biofilms caused elevated biofilm stiffness (stiffer biofilm, Fig. 8(b)).

Along with a decrease in biofilm thickness, a higher hydraulic biofilm resistance was measured after the biofilm was compacted, due to the reduction in porosity and the increase in the biofilm density. This indicates that biofilm compaction created a more compact biofilm with the same amount of biomass in a smaller volume, caused by reduction of open spaces (voids) in the biofilm and/or restructuring of the EPS/biofilm. Biofilm compaction explains the observation that a thinner biofilm displays a higher hydraulic resistance than a thicker biofilm. It was demonstrated that EPS are responsible for the hydraulic resistance of biofilms [13]. Compaction results in an increase of EPS concentration. Thus, EPS concentration (and not biofilm thickness) is a dominant parameter for hydraulic permeability [11].

A decrease in permeate flux after the compaction stage caused the biofilm thickness to increase, and a decrease in hydraulic biofilm resistance was observed, indicating relaxation of the biofilm. A lower hydraulic biofilm resistance is caused by a less compact biofilm with the same amount of biomass in a larger volume (partial recovery of the original thickness). In other words, the biofilm behaves like a spring and relaxes after reduction of the pressure, occupying a larger volume with the same biomass. This leads to a reduction of EPS concentration and, thus, to a lower hydrodynamic resistance of the biofilm.

4.2. Timescale of compaction and relaxation

Both biofilm compaction and relaxation caused by permeate flux variations proved to be time-dependant processes, occurring in a time frame of seconds. The compaction process was considerably faster than the relaxation process. In this study, compaction occurred mainly in the first two seconds after a permeate flux increase was applied. When the initial flux was restored, the biofilm recovered 79% of its original thickness in a time frame of 10 s. Contrary to the results obtained in this study, in previously discussed literature [7], relaxation of biofilms appeared to be related to an "adaptation time," and thus, the (original) thickness recovered in a much longer time period. In the experiments of Ohl et al. [7], the biofilms completely recovered the original thickness within a period of 1 to 3 weeks, depending on the thickness of the biofilm. A thicker biofilm needed more time to adapt to new hydrodynamic conditions. The time frame found by Ohl et al. [7] is much longer than the results shown in this study. However, over a long period as found by Ohl et al. [7], it may be difficult to discriminate between biofilm decompaction and biofilm growth.

4.3. Practical implications

The impact of biofilm accumulation on membrane performance is influenced by membrane module configuration, membrane plant design and operational aspects. A membrane system operated at a high or variable permeate flux may suffer from a compact biofilm formation, causing a high hydraulic resistance (high energy use and low permeate production). If the membrane system is operated at a low and constant permeate flux, the impact of biomass accumulating on membrane performance will be significantly lower.

When biofouling occurs in membrane systems, membrane cleaning is unavoidable. Based on the results from this study, effective cleaning strategies may be developed. When the biofilm is thicker and more porous, produced under low flux conditions, the cleaning agents may have a stronger impact on removing biofouling. This should be achieved by cleaning under low-flux/no-flux conditions in the membrane module.

Biofilm compaction and relaxation may also influence the effect of novel cleaning strategies. Two-phase flow cleaning in membrane processes has attracted interest [26,32,33]. Air bubbles may have a higher impact on biofouling removal when the biofilm is thicker, more porous and less rigid. High-shear biofilms are more compact and have a higher cohesion strength (are stronger attached), resulting in a more difficult to remove biofilm, while relaxed biofilms may be easier to control by advanced cleaning strategies [26].

Large-scale seawater RO plants can be operated with regular (daily) shutdown cycles (i.e. to save electricity cost) [34]. The shutdown time allows biofilm relaxation, and consequently, membrane performance and impact on membrane cleaning may be improved.

Table 2
Overview of potential future studies on biofilm formation, morphology, compaction and relaxation in relation to spacer design, membrane performance and advanced cleaning strategies

Topics
(1) Role of crossflow velocity and permeate flux
(2) Role of feed spacers and hydrodynamics
(3) Role of nutrients (type and concentration) and biofilm growth limiting nutrient (e.g. C or P) in feed water
(4) Role of hydraulic pressure
(5) Role of salt concentration and concentration polarization
(6) Spatial biofilm thickness and density in relationship to spatial permeate flux
(7) Relationship biofilm attachment strength and cleanability in relation to biofilm morphology, compaction and relaxation, spacer design and membrane operation parameters
(8) Longer term experiments to better predict implications for membrane systems applied in practice

4.4. Future studies

A set of tools is available enabling a broad suite of potential future studies (Table 2) on biofilm formation, morphology, compaction and relaxation in relation to spacer design, membrane performance and advanced cleaning strategies, contributing to the development of advanced biofouling control strategies.

OCT, a non-destructive imaging technique, is a powerful tool to analyse the behaviour of biofilms in combination with a monitor with the same hydraulic condition as full-scale installations providing sensitive and accurate membrane performance data.

At high crossflow velocity, a compact well-attached biofilm was obtained while a low crossflow caused a more fluffier, less-attached biofilm [26]. The biofilm cohesion strength is related to hydrodynamics. Clearly, there is a matrix of (interacting) parameters, influencing the extent and/or timescale of biofilm compaction and relaxation. In addition, differences in microbial biofilm communities may be affecting compaction and relaxation as well. In this study, the biofilm showed a broad thickness range over a small membrane area (Fig. 8). It is not clear whether the spatial biofilm thickness gradient caused variations in permeate flux (e.g. a high flux at a location with a relative thin biofilm and a low flux at a location with a thick biofilm). The consequences of biofilm thickness variations on local permeate flux and total hydraulic resistance may be studied for different biofilm thicknesses. Ongoing studies focus on the relationship between local biofilm thickness and permeate flux. It is not clear how biofilm compaction and relaxation with a very short timescale are related to membrane performance in long-term experiments. Future studies could address the impact of crossflow velocity and permeate flux on the formation, morphology, compaction and relaxation of biofilms and the impact on membrane performance. Feed spacers have shown to be of key importance for biofouling in spiral-wound membrane systems [25,35–37]. Modified spacer design may reduce the impact of biofilm accumulation on membrane performance.

A better understanding of biofilms and its impact on membrane performance may lead to development of more effective biofouling control strategies in full-scale membrane filtration installations applied for water treatment.

5. Conclusions

In situ biofilm thickness measurements using OCT were used to analyse the occurrence, extent and timescale of biofilm compaction and relaxation. Based on the results presented in this article on hydraulic biofilm resistance, biofilm thickness, biofilm thickness change rate, biofilm thickness range and biofilm stiffness, it can be concluded that:

(1) OCT measurements provided useful structural information (i.e. thickness) on biofilm compaction and relaxation in real time.
(2) An increase in water permeate flux resulted in biofilm compaction, decreasing the biofilm thickness and increasing the hydraulic biofilm resistance.
(3) The biofilm showed an increase in thickness during a relaxation stage (water flux restored to the original value).
(4) Biofilm thickness was partially recovered after compaction, by relaxation.

(5) The timescale for biofilm compaction and relaxation was in the order of seconds.
(6) Compaction occurred faster than relaxation.
(7) The biofilm showed a higher stiffness during and after compaction.
(8) In practice, these results indicate that permeate flux changes may lead to thinner biofilms with higher hydraulic resistance.

Supplemental material

The supplemental material for this article is available at http://dx.doi.org/10.1080/19443994.2015.1057036.

Acknowledgements

This work was performed at Wetsus, European Centre of Excellence for Sustainable Water Technology (www.wetsus.nl). Wetsus is funded by the Dutch Ministry of Economic Affairs, the European Union European Regional Development Fund, the Province of Fryslân, the city of Leeuwarden and by the EZ-KOMPAS Programme of the "Samenwerkingsverband Noord-Nederland." The work was funded by Wetsus, King Abdullah University of Science and Technology (KAUST) and Evides waterbedrijf. The authors like to thank the participants of the Wetsus research theme "Biofouling," KAUST and Evides waterbedrijf for the fruitful discussions and their financial support. In addition, the authors would especially like to thank the student Melvin Boelens for his great support with the experimental work in the laboratory.

References

[1] Z.-Y. Li, V. Yangali-Quintanilla, R. Valladares-Linares, Q. Li, T. Zhan, G. Amy, Flux patterns and membrane fouling propensity during desalination of seawater by forward osmosis, Water Res. 46(1) (2012) 195–204.
[2] H.C. Flemming, G. Schaule, T. Griebe, J. Schmitt, A. Tamachkiarowa, Biofouling—The achilles heel of membrane processes, Desalination 113(2–3) (1997) 215–225.
[3] W.G. Characklis, K.C. Marshall, Biofilms, John Wiley & Sons, New York, NY, 1990.
[4] C.S. Laspidou, B.E. Rittmann, Modeling the development of biofilm density including active bacteria, inert biomass, and extracellular polymeric substances, Water Res. 38(14–15) (2004) 3349–3361.
[5] P. Stoodley, Z. Lewandowski, J.D. Boyle, H.M. Lappin-Scott, Structural deformation of bacterial biofilms caused by short-term fluctuations in fluid shear: An *in situ* investigation of biofilm rheology, Biotechnol. Bioeng. 65(1) (1999) 83–92.
[6] E. Casey, Tracer measurements reveal experimental evidence of biofilm consolidation, Biotechnol. Bioeng. 98(4) (2007) 913–918.
[7] L. Ohl, H. Horn, D. Hempel, Behaviour of biofilm systems under varying hydrodynamic conditions, Water Sci. Technol. 49(11–12) (2004) 345–351.
[8] V. Körstgens, H.C. Flemming, J. Wingender, W. Borchard, Uniaxial compression measurement device for investigation of the mechanical stability of biofilms, J. Microbiol. Methods 46(1) (2001) 9–17.
[9] E. Paramonova, E.D. De Jong, B.P. Krom, H.C. Van Der Mei, H.J. Busscher, P.K. Sharma, Low-load compression testing: A novel way of measuring biofilm thickness, Appl. Environ. Microbiol. 73(21) (2007) 7023–7028.
[10] E. Paramonova, B.P. Krom, H.C. Van Der Mei, H.J. Busscher, P.K. Sharma, Hyphal content determines the compression strength of *Candida albicans* biofilms, Microbiology 155(6) (2009) 1997–2003.
[11] C. Dreszer, A.D. Wexler, S. Drusová, T. Overdijk, A. Zwijnenburg, H.C. Flemming, J.C. Kruithof, J.S. Vrouwenvelder, In-situ biofilm characterization in membrane systems using optical coherence tomography: Formation, structure, detachment and impact of flux change, Water Res. 67 (2014) 243–254.
[12] C. Dreszer, J.S. Vrouwenvelder, A.H. Paulitsch-Fuchs, A. Zwijnenburg, J.C. Kruithof, H.C. Flemming, Hydraulic resistance of biofilms, J. Membr. Sci 429 (2013) 436–447.
[13] C.S. Laspidou, L.A. Spyrou, N. Aravas, B.E. Rittmann, Material modeling of biofilm mechanical properties, Math. Biosci. 251 (2014) 11–15.
[14] A.F. Fercher, W. Drexler, C. K. Hitzenberger, T. Lasser, Optical coherence tomography-principles and applications. Rep. Prog. Phys. 2003 66(2) 239.
[15] N. Derlon, M. Peter-Varbanets, A. Scheidegger, W. Pronk, E. Morgenroth, Predation influences the structure of biofilm developed on ultrafiltration membranes, Water Res. 46(10) (2012) 3323–3333.
[16] N. Derlon, N. Koch, B. Eugster, T. Posch, J. Pernthaler, W. Pronk, E. Morgenroth, Activity of metazoa governs biofilm structure formation and enhances permeate flux during gravity-driven membrane (GDM) filtration, Water Res. 47(6) (2013) 2085–2095.
[17] C. Haisch, R. Niessner, Visualisation of transient processes in biofilms by optical coherence tomography, Water Res. 41(11) (2007) 2467–2472.
[18] D. Janjaroen, F. Ling, G. Monroy, N. Derlon, E. Mogenroth, S.A. Boppart, W.-T. Liu, T.H. Nguyen, Roles of ionic strength and biofilm roughness on adhesion kinetics of *Escherichia coli* onto groundwater biofilm grown on PVC surfaces, Water Res. 47(7) (2013) 2531–2542.
[19] C. Xi, D. Marks, S. Schlachter, W. Luo, S.A. Boppart, High-resolution three-dimensional imaging of biofilm development using optical coherence tomography. Biomedo 2006, 11(3) 034001-1–034001-6.
[20] Y. Gao, S. Haavisto, W. Li, C.Y. Tang, J. Salmela, A.G. Fane, Novel approach to characterizing the growth of a fouling layer during membrane filtration via optical coherence tomography, Environ. Sci. Technol. 48(24) (2014) 14273–14281.
[21] M. Wagner, D. Taherzadeh, C. Haisch, H. Horn, Investigation of the mesoscale structure and volumetric features of biofilms using optical coherence tomography, Biotechnol. Bioeng. 107(5) (2010) 844–853.

[22] J.S. Vrouwenvelder, S.M. Bakker, L.P. Wessels, J.A.M. Van Paassen, The membrane fouling simulator as a new tool for biofouling control of spiral-wound membranes, Desalination 204(1–3) (2007) 170–174.
[23] J.S. Vrouwenvelder, J.A.M. Van Paassen, L.P. Wessels, A.F. Van Dam, S.M. Bakker, The membrane fouling simulator: A practical tool for fouling prediction and control, J. Membr. Sci. 281(1–2) (2006) 316–324.
[24] C. Dreszer, H.C. Flemming, A.D. Wexler, A. Zwijnenburg, J.C. Kruithof, J.S. Vrouwenvelder, Development and testing of a transparent membrane biofouling monitor, Desalin. Water Treat. 52(10–12) (2014) 1807–1819.
[25] J.S. Vrouwenvelder, D.A. Graf von der Schulenburg, J.C. Kruithof, M.L. Johns, M.C.M. Van Loosdrecht, Biofouling of spiral-wound nanofiltration and reverse osmosis membranes: A feed spacer problem. Water Res. 2009, 433) 583–594.
[26] J.S. Vrouwenvelder, J. Buiter, M. Riviere, W.G.J. Van der Meer, M.C.M. Van Loosdrecht, J.C. Kruithof, Impact of flow regime on pressure drop increase and biomass accumulation and morphology in membrane systems, Water Res. 44(3) (2010) 689–702.
[27] J.S. Vrouwenvelder, F. Beyer, K. Dahmani, N. Hasan, G. Galjaard, J.C. Kruithof, M.C.M. Van Loosdrecht, Phosphate limitation to control biofouling, Water Res. 44(11) (2010) 3454–3466.
[28] G. Schock, A. Miquel, Mass transfer and pressure loss in spiral wound modules, Desalination 64 (1987) 339–352.
[29] N.A. Peppas, B.D. Barr-Howell, Characterization of the cross-linked structure of hydrogels, Hydrogels in medicine and pharmacy 1 (1986) 27–56.
[30] P.J. Flory, Theory of elasticity of polymer networks. The effect of local constraints on junctions, J. Chem. Phys. 66(12) (1977) 5720–5729.
[31] A. Sweity, W. Ying, M.S. Ali-Shtayeh, F. Yang, A. Bick, G. Oron, M. Herzberg, Relation between EPS adherence, viscoelastic properties, and MBR operation: Biofouling study with QCM-D, Water Res. 45(19) (2011) 6430–6440.
[32] Y. Wibisono, E.R. Cornelissen, A.J.B. Kemperman, W.G.J. Van der Meer, K. Nijmeijer, Two-phase flow in membrane processes: A technology with a future, J. Membr. Sci. 453 (2014) 566–602.
[33] E.R. Cornelissen, J.S. Vrouwenvelder, S.G.J. Heijman, X.D. Viallefont, D. Van Der Kooij, L.P. Wessels, Periodic air/water cleaning for control of biofouling in spiral wound membrane elements, J. Membr. Sci. 287(1) (2007) 94–101.
[34] A. Hermony, J.M. Pinto, New concept of upgrade energy recovery systems within an operating desalination plant. EuroMed, Desalination for Clean Water and Energy Cooperation among Mediterranean Countries 3-7 October 2010, Tel Aviv, Israel 1–14 (2010) 2010.
[35] S.A. Creber, J.S. Vrouwenvelder, M.C.M. Van Loosdrecht, M.L. Johns, Chemical cleaning of biofouling in reverse osmosis membranes evaluated using magnetic resonance imaging, J. Membr. Sci 362(1–2) (2010) 202–210.
[36] A.I. Radu, J.S. Vrouwenvelder, M.C.M. Van Loosdrecht, C. Picioreanu, Modeling the effect of biofilm formation on reverse osmosis performance: Flux, feed channel pressure drop and solute passage, J. Membr. Sci 365(1–2) (2010) 1–15.
[37] P.A. Araújo, J.C. Kruithof, M.C.M. Van Loosdrecht, J.S. Vrouwenvelder, The potential of standard and modified feed spacers for biofouling control, J. Membr. Sci 403–404 (2012) 58–70.